HSPI The Open Access Publisher

IJPRA ISSN 2766-2748 INTERNATIONAL JOURNAL OF PHYSICS RESEARCH AND APPLICATIONS

Research Article

Frequency-domain Characterization of Reverse Recovery Charge (QRR) in Commercial 1N4003 *pn*-Silicon Diodes

Mischa Robin Wieck[1], Stilianos Ouroumidis[2] and Andreas Dirk Wieck[2]*

[1]Hochschule Bochum, Fachbereich Elektrotechnik und Informatik, Am Hochschulcampus 1, D-44801 Bochum, Germany

[2]Chair of Applied Solid State Physics, Ruhr University Bochum, NB03/58, Universitätsstraße 150, D-44801 Bochum, Germany

More Information

***Address for correspondence:** Andreas Dirk Wieck, Chair of Applied Solid State Physics, Ruhr University Bochum, NB03/58, Universitätsstraße 150, D-44801 Bochum, Germany, Email: andreas.wieck@rub.de

Submitted: August 19, 2025
Approved: September 04, 2025
Published: September 05, 2025

How to cite this article: Wieck MR, Ouroumidis S, Wieck AD. Frequency-domain Characterization of Reverse Recovery Charge (QRR) in Commercial 1N4003 *pn*-Silicon Diodes. Int J Phys Res Appl. 2025; 8(9): 265-268. Available from: https://dx.doi.org/10.29328/journal.ijpra.1001134

Keywords: *pn*-Silicon diode; Reverse recovery charge; Frequency domain; Bandwidth limitation

Check for updates

OPEN ACCESS

Abstract

The reverse recovery charge (QRR) of silicon *pn* diodes is traditionally characterized in the time domain. In many technological applications—especially rectification of audio- and RF-range alternating currents—the frequency-domain manifestation of QRR is more relevant. We present a simple, analog frequency-sweep measurement method that reveals QRR-related limitations of rectification efficiency in real time. Using a sinusoidal excitation and oscilloscope frequency-axis mapping, we investigate the frequency ft at which the magnitude of the reverse current equals half that of the forward current. Measurements of 359 nominally identical 1N4003 diodes show a large spread in both forward voltage at 1,1 mA and ft , despite belonging to the same production batch. A Schottky diode reference (1N5711) shows no measurable reverse AC conduction within the tested range, confirming the method's validity. The approach provides a rapid and didactic alternative to conventional time-domain QRR measurements.

Introduction

The reverse recovery charge QRR in *pn*-junction diodes [1] is a key figure of merit for switching performance. Upon transitioning from forward to reverse bias, stored minority carriers in the depletion region must recombine or be swept out before the diode regains full blocking capability. In silicon *pn* diodes, the minority carrier lifetime in the depletion region—on the order of tens to hundreds of microseconds—is many orders of magnitude longer than the Drude scattering time of majority carriers, which is typically picoseconds. This long recombination time imposes significant limitations on the efficiency of high-frequency rectification.

While most QRR studies are conducted in the time domain by observing the reverse recovery current pulse after switching, applications in audio and RF rectification often benefit more from a frequency-domain perspective. The onset of significant reverse conduction manifests as a deterioration of rectification efficiency with increasing signal frequency, directly impacting signal integrity.

State of the Art

Standardized QRR measurement procedures [1,2] employ current-pulse or double-pulse methods to extract parameters such as reverse recovery time, $t_{rr,}$ and stored charge QRR. Time-domain techniques are essential for high-speed power electronics characterization, but can be cumbersome in low- and mid-frequency signal applications. They are described in detail in classical works and textbooks [3-5]. A detailed modeling [6], rectification efficiency optimization [7], a full-wave bridge rectifier [8], and GaN Schottky diodes parameters [9] have been performed. Then, GaN Schottky diodes [10], RF energy harvesting [11], high-frequency impedance [12], SiC MOSFET body-diodes [13], radio-frequency energy

harvesting [14], THz rectification [15], QRR reduction in SiC [16], 10-W-level microwave rectifier [17], RF PIN diodes [18], a modified finite-difference model [19], high-temperature applications [20], switching-loss estimation in a half-bridge [21], and suppressing the reverse-recovery [22] were under investigation. Furthermore, p-type Schottky diode embedded at the drain side for improved reliability [23], mitigating reverse recovery power losses [24], 1.2-kV SiC MOSFET body diode [25], achievable bandwidth [26], accurate diode behavioral model [27], multiepi superjunction [28], heterojunction diode-shielded SiC [29], punch-through n-p-n diode [30], high-temperature 4H-SiC MOSFETs [31], GHz rectifiers [32], comparison between Si, SiC and GaN [33] and class-E/F2 low-power RF rectifiers [34] were investigated. Practically all these research activities relate to time-domain experiments.

Frequency-domain approaches, although less common, offer advantages in audio electronics and instrumentation. By directly observing the rectification efficiency as a function of frequency, one can relate QRR effects to application-relevant bandwidth limits. This has been explored in specialized RF detector diode studies but is rarely applied to general-purpose rectifier diodes such as the 1N4003.

Experimental setup

We used a Hewlett-Packard HP3310A function generator to produce a 4 V amplitude sinusoidal signal applied to the anode (p-side) of the test diode. The cathode (n-side) was connected through a 1 kΩ resistor to ground. The voltage drop across the resistor, proportional to diode current, was fed to the Y-input of a Tektronix 7603 oscilloscope.

To obtain a frequency sweep on the oscilloscope's X-axis, the HP3310A frequency modulation (FM) input was driven with the oscilloscope's free-running sweep voltage. This setup allowed the generator's output frequency to be swept over approximately two decades during each oscilloscope trace (Figure 1). On the left, low-frequency side of the spectrum, we can follow the time evolution: After the first positive half-wave (forward direction of the diode), the trace goes straight to the negative current due to the QRR, crossing the zero current line. Then, this reverse current breaks down when the QRR is exhausted. The following positive half-wave shows again a full forward conduction, and since the frequency has been increased, this forward half-wave is shorter and the following reverse current peak as well. However, the same QRR charge has to be emptied, and the negative current peak is thus higher in a shorter time ($\int Idt$ being the constant QRR). In this way, the negative current peaks increase with increasing frequency to the right of the time scale. This occurs at higher frequencies up to saturation at higher frequencies, on the way crossing the absolute value of half the forward current, occurring in Figure 1 at 26 kHz. Interestingly, we mix here the frequency domain

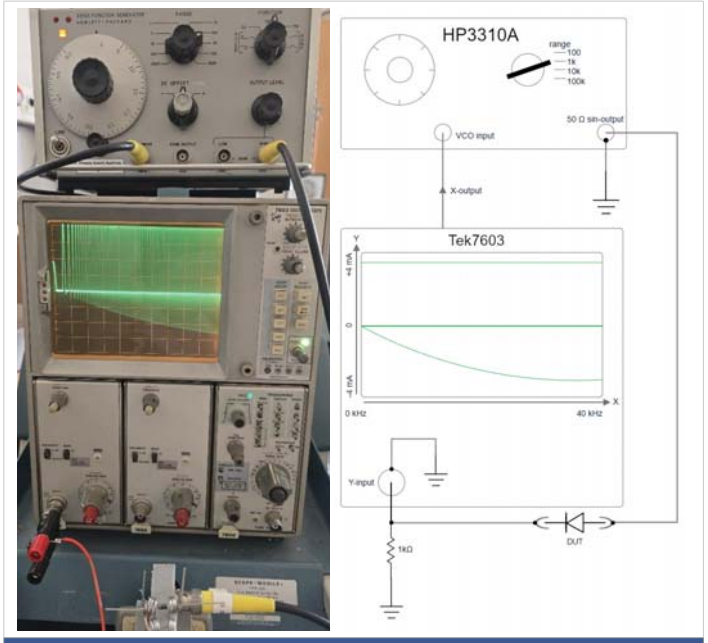

Figure 1: Left: Photograph of the actual setup with a 1N4003-pn-diode. Right: Symbolic wiring of the instruments and circuit drawing of the device under test (DUT). The frequency on the left of the oscilloscope screen is close to zero (individual half-waves visible) and increases linearly with 4kHz/div to 40kHz on the right side of the screen. The actual inserted diode 1N4003 exhibits f_t = 26 kHz.

with the time domain, the time base being 1ms / div in this case (the first positive half-wave having a length of about 0,2 ms, corresponding to 2,5 kHz). We will discuss this behavior in a subsequent paper.

We measured the forward voltage V_{fwd} in the "diode mode" of the multimeter OW18B (OWON), which injects a constant current of 1,1 mA and displays V_{fwd} in mV.

Key features of the method:

- **Positive half-cycles:** Appear above the zero Y-line.
- **Negative half-cycles:** Ideally absent for a perfect diode; appear below zero when reverse conduction occurs.
- **Half-point frequency f_t:** Defined where $|I_{rev}|=0.5\cdot I_{fwd}$.

The coarse frequency decade multiplier switch of the HP3310A was adapted to include f_t of each diode within a full frequency sweep, in most cases × 1 kHz to sweep between zero and 40kHz.

Results

Frequency sweeps

At low frequencies (a few Hz to hundreds of Hz), the negative half-wave amplitude was negligible, as expected for a functioning rectifier. As frequency increased, reverse conduction grew steadily due to incomplete carrier recombination. The transition from nearly ideal rectification to significant reverse conduction occurred over roughly one frequency decade.

Schottky diode reference

A Schottky diode 1N5711 (with typical minority carrier lifetime < 1 ns) exhibited no measurable reverse conduction in the tested range and above, up to 4 MHz, validating that the observed negative half-waves in pn-diodes originate from QRR (Figure 2).

Forward bias *vs.* $1/f_t$

Measurements of 359 commercial 1N4003 diodes from the same production batch revealed:

- **Forward DC voltage at 1,1 mA:** Scatter of about ±20 - 50 mV around the nominal 0.575 V.
- **Half-point frequency f_t:** Ranging from a few kHz to several hundred kHz.
- **Reverse leakage at DC −5 V:** From ≈1 nA to ≈ 100 nA.

A weak but noticeable correlation existed between higher forward voltage V_{fwd} and higher $1/f_t$, suggesting higher stored charge in higher-V_{fwd} devices.

Discussion

The broad scatter in f_t and leakage currents indicates significant variability in minority carrier lifetime and junction geometry, even within a single manufacturing batch. This is consistent with the indirect bandgap nature of silicon, where radiative recombination is inefficient, and defect-assisted nonradiative recombination dominates. Small differences in doping, defect density, or passivation can alter lifetime and thus QRR.

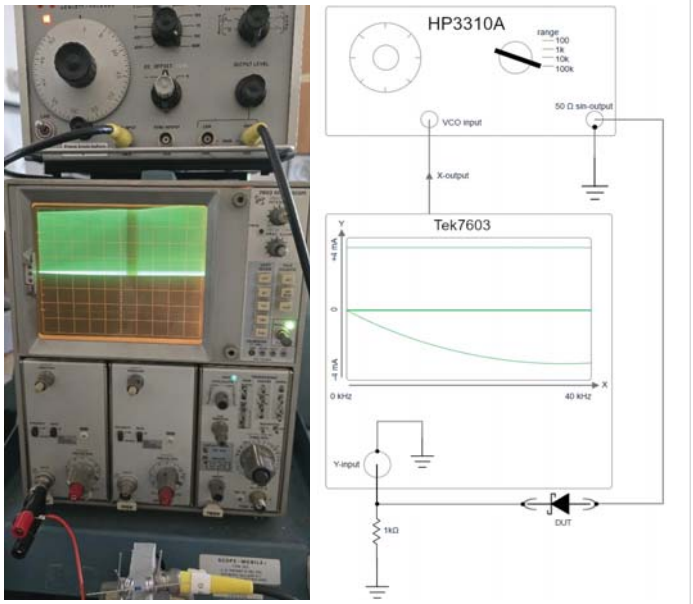

Figure 2: Left: Photograph of the setup with the Schottky-diode 1N5711 inserted as DUT. The frequency on the left of the oscilloscope screen is close to zero and increases linearly with 400 kHz/div to 4 MHz on the right side of the screen. Since there is no QRR, negative currents in the lower half of the screen are absent. The dark vertical stripe at ≈ 2,2 MHz is an artefact due to the overlay between the time sweep of the oscilloscope and the digital camera with which the photograph was shot. Right: Schematics of the setup.

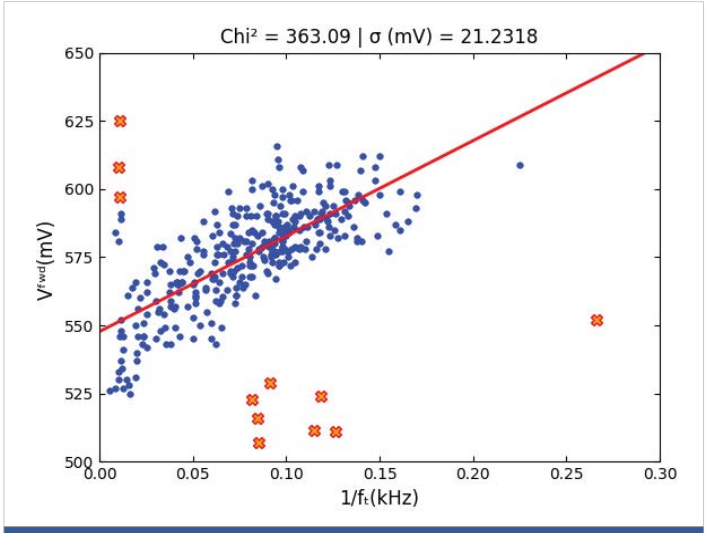

Figure 3: Forward voltage V_{fwd} versus $1/f_t$. The measured values outside of 2σ = 42,5 mV deviation from the red regression line are marked with red ✖ es.

The higher the forward voltage V_{fwd} is, the higher is also the *p* and *n* doping density. Thus, there are more electron-hole pairs in the depletion zone, and it takes longer to empty it, i.e., the inverse frequency $1/f_t$ rises with increasing V_{fwd}. In assuming a simple proportional increase as a first guess, we evaluate a regression line in Figure 3, which roughly describes this dependence. To model it more precisely, theoretical efforts are needed, which, however, may not make much sense in view of the heavy scatter in this batch.

Only 11 samples of 359 (3%) are not in this trend; further investigations are underway to figure out whether they are unusual diodes in practice.

The frequency-domain method demonstrated here is not a replacement for standardized QRR characterization in power device engineering, but it is:

- Highly intuitive for understanding rectification limits.
- Rapid for screening large batches.
- Directly relevant for low- and mid-frequency applications such as audio rectifiers.

Conclusion

We have demonstrated a simple, didactic, and versatile frequency-domain method for assessing the QRR-related frequency limit f_t of silicon *pn* diodes. Large spreads in both V_{fwd} and f_t were observed in 1N4003 diodes from a single batch, underscoring the benefit of diode selection for frequency-critical applications. This method bridges the gap between lab-grade QRR characterization and practical needs in audio and RF electronics, enabling efficient in-situ component screening.

Acknowledgement

We thank Prof. Dr. Jean-Yves Duboz from the CRHEA-CNRS in Sophia-Antipolis / France, for valuable discussions.

References

1. JEDEC Solid State Technology Association. Measurement of Reverse Recovery Time of Power Diodes. JESD282-B. Arlington, VA: JEDEC; 2011.
2. International Electrotechnical Commission. Semiconductor devices – Discrete devices – Part 2: Rectifier diodes. IEC 60747-2. Geneva: IEC; 2016.
3. Sze SM, Ng KK. Physics of Semiconductor Devices. 3rd ed. Hoboken (NJ): Wiley; 2007. Available from: https://www.scirp.org/reference/referencespapers?referenceid=1703614
4. Moll JL, Haynes JR, Johnston CW. P-N junction switching. Proc IRE. 1958;46(6):1076–1081.
5. Schroder DK. Semiconductor Material and Device Characterization. Hoboken (NJ): Wiley; 2006. Available from: https://www.optima.ufam.edu.br/SemPhys/Downloads/Dieter.pdf
6. Casolaro P, Izzo VV, Giusi GG, Wyrsch NN, Aloisio A. Modeling the diffusion and depletion capacitances of a silicon pn diode in forward bias with impedance spectroscopy. J Appl Phys. 2024;136(11):115702. Available from: https://doi.org/10.1063/5.0230008
7. Gyawali B, Thapa SK, Barakat A, Yoshitomi K, Pokharel RK. Analysis and design of diode physical limit bandwidth efficient rectification circuit for maximum flat efficiency, wide impedance, and efficiency bandwidths. Sci Rep. 2021;11:19941. Available from: https://www.nature.com/articles/s41598-021-99405-7
8. Liang TY, Zakaria NF, Kasjoo SR, Shaari S, Isa MM, Md Arshad MK, Singh AK. Silicon Self-Switching Diode (SSD) as a full-wave bridge rectifier in 5G networks frequencies. Sensors. 2022;22(24):9712. Available from: https://doi.org/10.3390/s22249712
9. Muhammad S, Waly MI, AlJarallah NA, Ghayoula R, Negm AS, Smida A, et al. A multiband SSr diode RF rectifier with an improved frequency ratio for biomedical wireless applications. Sci Rep. 2023;13:13246. Available from: https://doi.org/10.1038/s41598-023-40486-x
10. Orfão B, Abou-Daher M, Zegaoui M, Mateos J, González T, Okada E, et al. GaN Schottky diodes parameter extraction model from S-parameters measurement. In: Proceedings of the 19th European Microwave Integrated Circuits Conference (EuMIC); 2024. p. 375. Available from: https://doi.org/10.23919/EuMIC61603.2024.10732802
11. Reddaf A, Boudjerda M, Bouchachi I, Babes B, Elrashidi A, AboRas KM, Ali E, Ghoneim SSM, Elsisi M. Modeling of Schottky diode and optimal matching circuit design for low power RF energy harvesting. Heliyon. 2024;10:e27792. Available from: https://doi.org/10.1016/j.heliyon.2024.e27792
12. van Nijen DA, Procel P, van Swaaij RACMM, Zeman M, Isabella O, Manganiello P. The nature of silicon PN junction impedance at high frequency. Sol Energy Mater Sol Cells. 2025;282:113383. Available from: https://doi.org/10.1016/j.solmat.2024.113383
13. Pennisi G, Pulvirenti M, Salvo L, Sciacca AG, Cascino S, Laudani A, Salerno N, Rizzo RS, Rizzo SA. Investigation of SiC MOSFET body-diode reverse recovery and snappy recovery conditions. Energies. 2024;17:2651. Available from: https://doi.org/10.3390/en17112651
14. Zhang A, Grajal J, López-Vallejo M, McVay E, Palacios T. Opportunities and challenges of ambient radio-frequency energy harvesting. Patterns. 2020;1:100089. Available from: https://doi.org/10.1016/j.patter.2020.100089
15. Citroni R, Pucci AR, Cojoc D, Dickmann F, Decker A. Progress in THz rectifier technology: research and perspectives. Nanomaterials. 2022;12:2479. Available from: https://doi.org/10.3390/nano12142479
16. Wang X, Yu Q, Chen L, Li Y, Zhou P. Qrr reduction in SiC MOSFET structures: experimental and TCAD study. Microelectron J. 2024;126:105798.
17. Peng H, Gao Y, Huang L, Liu J. 10-W-level microwave rectifier: large-signal S-parameter evaluation. Electronics. 2024;13:2024. Available from: https://doi.org/10.3390/electronics13020423
18. Botha CJ, Stander T. The effect of temperature variation on the transient response of RF PIN diode limiters for very high frequency applications. IET Microw Antennas Propag. 2024;18:849. Available from: https://doi.org/10.1049/mia2.12508
19. Zhang M. A modified finite-difference model to the reverse recovery of silicon PIN diodes. Solid-State Electron. 2020;171:107839. Available from: https://doi.org/10.1016/j.sse.2020.107839
20. Qian C, Wang Z, Zhou D, Ge Y, Zhou Y, Xin X, Shi X. Investigation of reverse recovery phenomenon for SiC MOSFETs in high-temperature applications. IEEE Trans Power Electron. 2023;38:14375. Available from: https://doi.org/10.1109/TPEL.2023.3273351
21. Nayak DP, Yakala RK, Kumar M, Pramanick SK. Temperature-dependent reverse recovery characterization of SiC MOSFETs' body diode for switching-loss estimation in a half-bridge. IEEE Trans Power Electron. 2022;37:5574. Available from: https://doi.org/10.1109/TPEL.2021.3128947
22. Shu J, Sun J, Zheng Z, Chen KJ. Suppressing the reverse-recovery of Si super-junction MOSFET with a low-voltage GaN HEMT in a cascode configuration. In: Proceedings of the 35th International Symposium on Power Semiconductor Devices and ICs (ISPSD); 2023. Available from: https://doi.org/10.1109/ISPSD57135.2023.10147632
23. Pavan P, Vudumula V, Kotamraju SS, Prasad LLVD, Ramasamy S. Reverse-recovery characteristics of an SiC superjunction MOSFET with a p-type Schottky diode embedded at the drain side for improved reliability. J Comput Electron. 2021;20:548.
24. Bououd M, Lai Y, Voldoire A, Hoang E, Béthoux O. Mitigating reverse recovery power losses in MOSFET switching cell using extra Schottky diodes — application to voltage-source inverter. Power Electron Devices Components. 2024;100066. Available from: https://doi.org/10.1016/j.pedc.2024.100066
25. Xue Z, Zhu M, Cui H, Yang F, Pei Y, Wang L. TCAD modeling of temperature-dependent reverse recovery characteristics of 1.2-kV SiC MOSFETs' body diode. In: Proceedings of the IEEE Energy Conversion Congress and Exposition (ECCE); 2023. Available from: https://doi.org/10.1109/ECCE53617.2023.10362165
26. Zhang X, Xu B, Li C, Zhao D, Chen E. RF-to-DC conversion limits: device capacitances, series resistance and achievable bandwidth. IEEE Trans Power Electron. 2024;39:4567.
27. Zhang M, Banáš S. Accurate diode behavioral model with reverse recovery. Solid-State Electron. 2020;171:107839.
28. Hua M, Cai X, Yang S, Zhang Z, Wang N, Chen KJ. A multiepi superjunction MOSFET with a lightly doped MOS-channel diode for improving reverse recovery. IEEE Trans Electron Devices. 2021;68:2401.
29. An A, Hu S. Heterojunction diode-shielded SiC split-gate trench MOSFET with optimized reverse-recovery characteristic and low switching loss. IEEE Access. 2019;7:28592–28596. Available from: https://doi.org/10.1109/ACCESS.2019.2902246
30. Peng X, Liu Y, Feng H, Zhang Q, Wang B. Analysis and characterization of the punch-through n-p-n diode for hard-switching power control applications. IEEE Trans Electron Devices. 2023;70:4525–4531. Available from: https://doi.org/10.1109/TED.2023.3294358
31. Potbhare S, Goldsman N, Lelis A, McGarrity JM, McLean FB, Habersat D. A physical model of high-temperature 4H-SiC MOSFETs including reverse-recovery effects. IEEE Trans Electron Devices. 2022;69:2022.
32. Zhang F, Li J, Wang R, Zhao S, Chen X. S-parameter based small-signal extraction of diode nonlinear capacitances for GHz rectifiers. IEEE Microw Wireless Compon Lett. 2023;33:145.
33. Peng P, Zhou H, Sun L, Wang Y. Modeling of device-level reverse recovery dynamics with TCAD: comparison between Si, SiC and GaN. Solid-State Electron. 2024;200:108496.
34. Mansour A, Elshafai F, Abouissa M, ElHussieny H. Class-E/F2 low-power RF rectifiers: rectification behaviour and DC-output versus frequency. Microelectron Eng. 2023;272:111794.